

Ultrahigh- Q silicon resonators in a planarized local oxidation of silicon platform

Alex Naiman,* Boris Desiatov, Liron Stern, Noa Mazurski, Joseph Shappir, and Uriel Levy

Department of Applied Physics, The Benin School of Engineering and Computer Science, The Center for Nanoscience and Nanotechnology, The Hebrew University of Jerusalem, Jerusalem 91904, Israel

*Corresponding author: alex.naiman@mail.huji.ac.il

Received January 16, 2015; revised February 15, 2015; accepted February 16, 2015;
posted February 17, 2015 (Doc. ID 232362); published April 17, 2015

We describe a platform for the fabrication of smooth waveguides and ultrahigh-quality-factor (Q factor) silicon resonators using a modified local oxidation of silicon (LOCOS) technique. Unlike the conventional LOCOS process, our approach allows the fabrication of nearly planarized structures, supporting a multilayer silicon photonics configuration. Using this approach we demonstrate the fabrication and the characterization of a microdisk resonator with an intrinsic Q factor that is one of the highest Q factors achieved with a compact silicon-on-insulator platform. © 2015 Optical Society of America

OCIS codes: (140.3945) Microcavities; (140.4780) Optical resonators; (220.4000) Microstructure fabrication; (230.4000) Microstructure fabrication; (230.7020) Traveling-wave devices; (130.0250) Optoelectronics.

<http://dx.doi.org/10.1364/OL.40.001892>

Silicon photonics presents itself as a promising platform for multiple applications, e.g., optical communications, nonlinear optics, and biochemical sensing. The virtue of silicon lies in its high refractive index, allowing tight confinement of light with the outcome of miniaturization of optical components, enhanced light-matter interactions, and reduced power consumption. Given its compatibility with the current CMOS fabrication process, silicon photonics technology allows for a drastic reduction in the cost of optical components and systems. Typically, most photonic devices are fabricated in a planar fashion, with all the components residing at a single plane. Yet, the possibility of using a multiplane scheme for waveguide crossings, modulators, switches, and photodetectors has been proposed [1] and demonstrated [2,3]. One of the main difficulties in implementing a multi-layer design lies in the ability to planarize the lower device plane in preparation for the device to be fabricated at the top plane. One way to address this issue is by spin coating the bottom plane devices with a fluid-like oxide, which produces a semiflat surface with a bump on top of the silicon, a procedure that can be used for some applications with a more relaxed demand for planarization. The most common scheme for obtaining surface planarization is chemical mechanical polishing (CMP), a method that combines mechanical polishing with the addition of a chemical slurry for the enhancement of particle removal, selectivity, and fine-tuning of the polishing process. Yet, CMP is an expensive process and requires careful control over its parameters. Furthermore, CMP makes use of a mechanical force to remove the material, and thus may result in strain and cracks in the polished layer. As an alternative, we propose and demonstrate the use of local oxidation of silicon (LOCOS) [4–6] combined with a preliminary short etching step in order to achieve planar silicon structures. As a by-product, the scattering loss of the fabricated devices is drastically reduced, allowing for optical resonators with ultrahigh quality factors (Q factors) to be achieved. Recently, several successful demonstrations of microring resonators fabricated using the LOCOS technique while achieving very high Q factors (up to $7.6 \cdot 10^5$) were reported [7–9].

Furthermore, this technology was utilized for the purpose of demonstrating frequency comb generation [10], and also for active plasmonic devices [11,12]. In our current work we demonstrate the benefit of the modified planar LOCOS method by the fabrication of whispering gallery mode (WGM) disk resonators. With this approach we were able to achieve an intrinsic Q factor of 5.3 million in 30 μm radius disk resonators. This is among the highest values achieved on a silicon-on-insulator (SOI) platform [13].

The resonators were fabricated on a commercial SOI wafer (SOITEC) with a 2 μm buried oxide layer and a 220 nm top silicon layer. The wafer was diced into 2 cm \times 2 cm chips. Next, a 200 nm silicon nitride layer was deposited on top using plasma-enhanced chemical vapor deposition (PECVD) as shown in Fig. 1(a), followed by the spin coating of a 250 nm thick layer of ZEP 520A electron beam lithography (EBL) resist. We then patterned the resist mask using EBL; see Fig. 1(b). The pattern was transferred to the silicon nitride and the silicon layers beneath with a single step of reactive ion etching (RIE) using a mixture of SF_6 and CHF_3 , as shown in Fig. 1(c). The silicon nitride was fully etched, while the silicon layer was partially etched. The key point is to precisely control the etching depth of the silicon layer such that after the consecutive step of oxidation (which expands the dimensions of the oxidized layer), the oxidized silicon (silicon dioxide) will compensate for the etching depth and will be at the same height as the unoxidized silicon, which was protected by the nitride layer. As a result, a planar top surface is achieved. The required silicon etch depth is given by

$$h^f = \frac{N^{\text{SiO}_2}}{N^{\text{Si}}} h^i = \frac{2.3 \cdot 10^{22} [\text{molecules}/\text{cm}^3]}{5 \cdot 10^{22} [\text{atoms}/\text{cm}^3]} 220 [\text{nm}] \approx 101 [\text{nm}]. \quad (1)$$

$h^{i,f}$ are the initial (220 nm in our case) and final (after the RIE step) silicon heights, respectively. The molecular density of silicon oxide and the atomic density of silicon

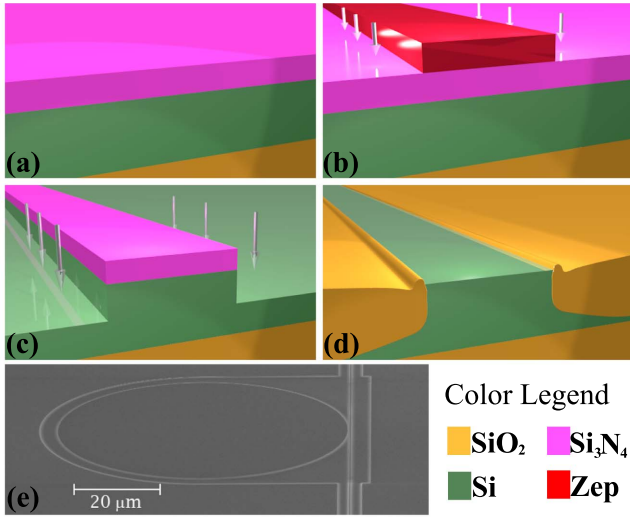


Fig. 1. Schematic description of the fabrication process. (a) Deposition of 100 nm thick layer of Si_3N_4 using PECVD on top of a 220 nm SOI, (b) waveguide patterning in ZEP e-beam resist by EBL, (c) dry etching of the silicon nitride and partial etching of the silicon layer, (d) wet oxidation of the silicon and removal of the nitride layer by a phosphoric acid solution, (e) SEM image of the disk resonator side coupled to a waveguide.

are denoted as N^{SiO_2} and N^{Si} , respectively. After the etching step, the electroresist was removed by a 10 min dip in ZEP remover (ZDMAC) at 80°C, followed by a Piranha ($\text{H}_2\text{SO}_4:\text{H}_2\text{O}_2$, 3:1) cleaning for 15 min. The wet oxidation step was performed in an oxidation furnace with a constant flow of distilled water steam at 920°C for 130 min, which resulted in oxidation of the silicon that was not protected by the silicon nitride layer. Finally, we removed the remaining silicon nitride layer by wet etch in hot phosphoric acid at 160°C for 50 min. After the nitride etch, another Piranha step was performed for 15 min. The end result was a planar and smooth structure, as can be seen schematically in Fig. 1(d). A scanning electron microscope (SEM) image of the fabricated structure is shown in Fig. 2(b). For the characterization of the surface planarity, we scanned the surface with an atomic force microscope (AFM), as can be seen in Fig. 2(a). The planar structure is evident, except for the small

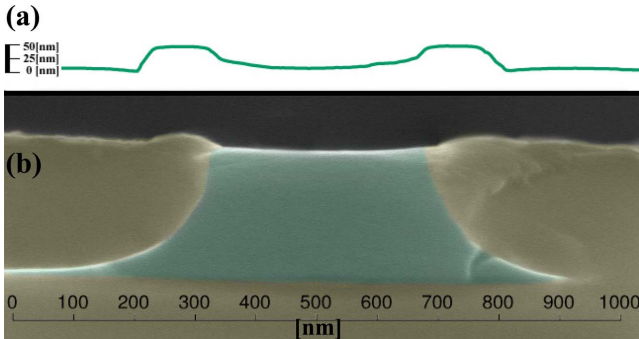


Fig. 2. (a) AFM scan of the surface of a planar LOCOS waveguide, (b) SEM image of a planar LOCOS waveguide; false colors used for emphasis, green for Si and yellow for SiO_2 . (The x and y scale are the same for the two figure parts.)

oxide bumps at the sides of the waveguide. These bumps are about 150 nm in width and 50 nm in height. Even though the surface is not fully planar yet, the volume of the nonplanar region is about 500 times smaller than the original volume of the disk. The dimensions of the bump can be reduced by further process optimization, e.g., using higher oxidation temperatures, which leads to reduced oxide viscosity [14] and more fluid-like behavior of the oxide.

Following the device fabrication, we turn to its experimental characterization. The experimental setup is shown in Fig. 3. It consists of a tunable laser (Agilent 81680A) in the range of 1460–1580 nm. The laser is coupled to the chip in an “end fire” configuration using a polarization-conserving lensed fiber (OZ Optics) and outcoupled using another lensed fiber to a GaInAs detector (Agilent 81634B). In order to obtain high spectral resolution, which is needed for the detection of narrow resonances, we applied a varying voltage of ± 5 V on the analog input of the laser for a fine wavelength tunability of ± 75 pm. The signal from the detector was then collected using a data acquisition card (National Instruments 6211) with a resolution of $\Delta\lambda = 0.037$ pm. This resolution is sufficiently high to allow the characterization of extremely narrow resonances, with a Q factor in the range of a million and above. The device on which we performed our measurements consists of a single-mode waveguide, which supports the fundamental TE mode with an effective refractive index of 2.32 for a resonance wavelength 1480 nm. It is 350 nm wide at the top and 520 nm wide at its bottom. The waveguide is side coupled to a 30 μm radius disk resonator, with an ~ 250 nm gap between them. In practice, the device was slightly over-etched, leading to the formation of small oxide shoulders, as can be seen in the inset of Fig. 4. These shoulders can be avoided by further process optimization. The highest Q factor was obtained for a resonance wavelength around $\lambda = 1480.5$ nm, and it can be seen in Fig. 4 as well, together with the Lorentzian fit. The intrinsic Q factor can be calculated [13] as $Q_i = 2Q_{\text{loaded}}/(1 + \sqrt{T_{\text{min}}})$, where Q_i is the intrinsic Q factor and Q_{loaded} is the actual Q factor, including the coupling loss between the resonator and the adjacent waveguide. T_{min} is the normalized power measured at the resonance. Based on the data presented in Fig. 4, we obtain an intrinsic Q factor of $Q_i = 5.33 \cdot 10^6$, which is among the highest values reported so far for such a small disk radius in an SOI platform. The reported resonance is one out of a total of 170 resonances that have been observed. These resonances appear with different Q factors and extinction ratios in a

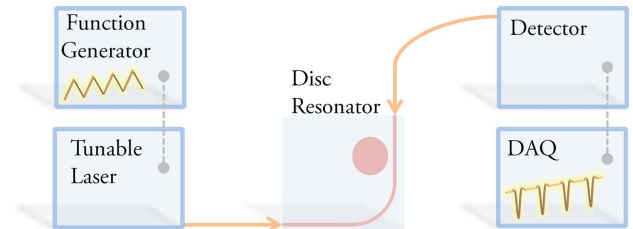


Fig. 3. Schematic diagram of the experimental setup used for the device characterization.

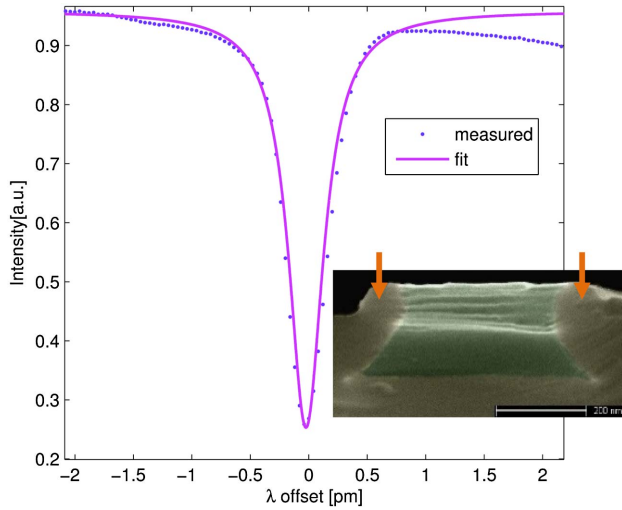


Fig. 4. Measured transmission spectrum of the device, showing a resonance around 1480.5 nm with a loaded Q factor of 4 million and extinction ratio of 6 dB. A Lorentzian fit is also provided. The inset shows an SEM image of the measured device with small oxide shoulders, emphasized by the orange arrows. False colors used for emphasis, green for Si and yellow for SiO_2 .

wavelength range of 1480–1580 [nm]. Based on a finite element method simulation (COMSOL Multiphysics) of the disk resonator, there are about 30 resonances for each radial mode in our working wavelength range, with a free spectral range of ~ 2.7 nm. From the experimental results, we believe that at least five of these radial modes are evident. Due to the reduced field overlap between the high-radial-order modes and the side silicon-oxide interface of the disk, we believe that it is the higher order modes that are associated with the high- Q -factor resonances. Our measurements show that 55 out of the 170 resonances have extinction ratios above 3 dB, together with a high Q factor of over a million. Therefore, the high- Q resonances can be correlated with reduced surface absorption and surface roughness due to the nature of the fabrication process, which will be rigorously analyzed in the following paragraph.

Finally, we discuss the physical mechanisms that determine the Q factor of our device. Over the last decade and a half there have been several demonstrations of ultrahigh- Q -factor resonators reaching up to nearly $Q = 10^{10}$ in relatively large ($R = 350$ μm) fused silica microspheres (see, e.g., [15]). An effort has been made to reduce the size of the resonators while still reaching high Q factors using microtoroids on a chip [16–18], photonic crystal microcavities [19–21], and WGM planar disk resonators [3,22,23], such as the one in this work. In order to understand the physical mechanisms limiting the Q factor in our work, we examine each of these mechanisms in more detail, following the discussions in [13,23]. The overall Q factor is given by

$$[Q_i]^{-1} = [Q_r^{-1} + Q_{b,\text{abs}}^{-1} + Q_{s,\text{abs}}^{-1} + Q_{\text{scat}}^{-1}] + [Q_{\text{TPA}}^{-1} + Q_{\text{TPA,FC}}^{-1}]. \quad (2)$$

Q_i is the intrinsic Q factor of the unloaded resonator. It consists of two main contributions, linear (left brackets)

and nonlinear (right brackets). The linear contribution consists of Q_r , which is related to loss due to radiation and is mainly affected by the bending loss; $Q_{b,\text{abs}}$, which is related to the absorption of the bulk material; $Q_{s,\text{abs}}$, which is related to surface absorption due to lattice reconstruction at the lateral edges of the resonator at the transition from Si to the thermal oxide; and Q_{scat} , which is related to the Rayleigh scattering by the coupling of the resonator modes to radiating modes due to surface roughness. The term on the right represents the nonlinear contribution, and it consists of Q_{TPA} , which is related to the loss due to two-photon absorption (TPA), and $Q_{\text{TPA,FC}}$, which is related to the loss due to TPA-induced free carrier absorption. Both can be neglected at a low power regime, as was applied in our measurements. Thus, we focus on the term on the left in Eq. (2). We start with Q_r , which is well above 10^7 even for smaller disks with a radius of 3 μm [13], and thus is not likely to be the limiting factor in our case. Q_{scat} is not likely to be the limiting factor either. This is because the scenario of high scattering due to surface roughness results in the coupling of radiated energy to the mode propagating in the opposite direction, leading to resonance splitting. Yet, resonance splitting was only observed in 5 out of 170 resonances. We are left with $Q_{b,\text{abs}}$ and $Q_{s,\text{abs}}$. While we did not differentiate between the two, it is reasonable to assume that $Q_{s,\text{abs}} < Q_{b,\text{abs}}$ because of the lattice defects at the edges of the silicon, leading to higher absorption at the surface. The bulk absorption can be calculated from the resistivity measurements of the bulk silicon [24]. The resistivity of the Si used in this work was 8.5–11.5 $[\Omega \cdot \text{cm}]$, resulting in $Q_{b,\text{abs}} > 3 \cdot 10^7$. Therefore, surface absorption is probably the mechanism limiting the Q factor. Considering the fact that we observed resonances with $Q_i > 5 \cdot 10^6$, we believe that our result is not far from the maximal achievable Q in our system. Yet, a slight improvement may be further achieved by considering methods for surface treatment and incorporating techniques borrowed from the discipline of surface chemistry (see, e.g., [25]).

To summarize, we demonstrated a method for the fabrication of smooth and planar photonic silicon devices in an SOI platform. Using this method we have fabricated WGM disk resonators with a Q factor as high as 5.33 million, which is among the highest values achieved in an SOI platform. This result demonstrates the advantage of our fabrication method for the construction of high-quality optical devices. Furthermore, the nearly flat structures being achieved by this method allow for the fabrication of additional photonic layers on top. By doing so, further improvement in photonic circuitry density can be achieved.

References

1. A. Biberman, N. Sherwood-Droz, X. Zhu, K. Preston, G. Hendry, J. S. Levy, J. Chan, H. Wang, M. Lipson, and K. Bergman, *Proc. SPIE* **7942**, 79420M (2011).
2. N. Sherwood-Droz and M. Lipson, *Opt. Express* **19**, 17758 (2011).
3. Q. Li, A. A. Eftekhari, M. Sodagar, Z. Xia, A. H. Atabaki, and A. Adibi, *Opt. Express* **21**, 18236 (2013).
4. L. K. Rowe, M. Elsey, N. G. Tarr, A. P. Knights, and E. Post, *Electron. Lett.* **43**, 392 (2007).

5. B. Desiatov, I. Goykhman, and U. Levy, *Opt. Express* **18**, 18592 (2010).
6. J. Cardenas, C. B. Poitras, J. T. Robinson, K. Preston, L. Chen, and M. Lipson, *Opt. Express* **17**, 4752 (2009).
7. L.-W. Luo, G. S. Wiederhecker, J. Cardenas, C. Poitras, and M. Lipson, *Opt. Express* **19**, 6284 (2011).
8. M. P. Nezhad, O. Bondarenko, M. Khajavikhan, A. Simic, and Y. Fainman, *Opt. Express* **19**, 18827 (2011).
9. A. Griffith, J. Cardenas, C. B. Poitras, and M. Lipson, *Opt. Express* **20**, 21341 (2012).
10. A. G. Griffith, R. K. Lau, J. Cardenas, Y. Okawachi, A. Mohanty, C. Poitras, A. L. Gaeta, and M. Lipson, in *CLEO: 2014 Postdeadline Paper Digest*, OSA Technical Digest (online) (Optical Society of America, 2014), paper STh5C.6.
11. A. Emboras, I. Goykhman, B. Desiatov, N. Mazurski, L. Stern, J. Shappir, and U. Levy, *Nano Lett.* **13**, 6151 (2013).
12. I. Goykhman, B. Desiatov, J. Khurgin, J. Shappir, and U. Levy, *Nano Lett.* **11**, 2219 (2011).
13. M. Borselli, T. Johnson, and O. Painter, *Opt. Express* **13**, 1515 (2005).
14. D.-B. Kao, J. P. McVittie, W. D. Nix, and K. C. Saraswat, *IEEE Trans. Electron Devices* **35**, 25 (1988).
15. D. W. Vernooy, V. S. Ilchenko, H. Mabuchi, E. W. Streed, and H. J. Kimble, *Opt. Lett.* **23**, 247 (1998).
16. H. Lee, T. Chen, J. Li, K. Y. Yang, S. Jeon, O. Painter, and K. J. Vahala, *Nat. Photonics* **6**, 369 (2012).
17. T. Lu, H. Lee, T. Chen, S. Herchak, J.-H. Kim, S. E. Fraser, R. C. Flagan, and K. Vahala, *Proc. Natl. Acad. Sci.* **108**, 5976 (2011).
18. J.-B. Jager, V. Calvo, E. Delamadeleine, E. Hadji, P. Noé, T. Ricart, D. Bucci, and A. Morand, *Appl. Phys. Lett.* **99**, 181123 (2011).
19. Y. Lai, S. Pirotta, G. Urbinati, D. Gerace, M. Galli, M. Minkov, V. Savona, and A. Badolato, in *CLEO: 2014*, OSA Technical Digest (online) (Optical Society of America, 2014), paper SM4M.2.
20. D. Yang, H. Tian, and Y. Ji, in *CLEO: 2014*, OSA Technical Digest (online) (Optical Society of America, 2014), paper JW2A.8.
21. H. Sekoguchi, Y. Takahashi, T. Asano, and S. Noda, *Opt. Express* **22**, 916 (2014).
22. M. Soltani, S. Yegnanarayanan, Q. Li, A. A. Eftekhar, and A. Adibi, *Phys. Rev. A* **85**, 053819 (2012).
23. M. Soltani, Q. Li, S. Yegnanarayanan, and A. Adibi, *Opt. Express* **18**, 19541 (2010).
24. R. A. Soref and B. R. Bennett, *IEEE J. Quantum Electron.* **23**, 123 (1987).
25. M. Borselli, T. J. Johnson, and O. Painter, *Appl. Phys. Lett.* **88**, 131114 (2006).